Additive manufacturing of bionanomaterials for biomedical applications based on TI6AL4V and PLA: a systematic review

Hatice Evlen[1,2*], *Umida* Ziyamukhamedova[2,1], *Dilmurod* Juraev[1], and *Mirzohid* Abdukarimov[3]

[1]Karabuk University, Turkey
[2]Tashkent State Transport University, Tashkent, Uzbekistan
[3]Tashkent State Technical University Named after Islam Karimov, Tashkent, Uzbekistan

Abstract. Additive manufacturing (AM) is the owner of a huge potential as a manufacturing technology in fabricating functional implants, and scaffolds for biomedical applications. AM, which includes 3D printing (3DP) and 3D bioprinting, can be the solution to produce several needs such as scaffolds/implants, tissue or organs, or medical devices by combining different biomaterials with nanomaterials. Titanium and its alloys and Polylactic acid (PLA) are commonly used in bone tissue repair with their superior bio-functionality. The rapid advancement of three-dimensional (3D) printing technology has enabled the fabrication of porous titanium and polymer composite scaffolds with controllable microstructures, which is regarded as an effective method for promoting rapid bone repair. An electronic literature search was conducted in PubMed, Web of Science, Scopus, Elsevier, Embase, and other numerous databases up to December 2021 which are accessed by Karabuk university. To evaluate the possibility of bias and methodological quality, the SYRCLE tool and the last version of the CAMARADES list were used, respectively, a meta-analysis could not be performed. This systematic review is aimed to evaluate the common biomedical potential of 3D-printed porous Ti6Al4V (Ti64) and PLA matrix scaffold for repairing bone defects to investigate the influential factors that might affect its osteogenic availability. The most ideal parameters for designing the Ti64 scaffold were found to be a pore size of around 300-400 m and porosity of 60-70%, while PLA scaffolds show 350-400 m and nearly the same percentage in porosity as Ti64.

1 Introduction

Repairing of tissues is considered an interesting subject in research, especially in orthopedic fields. It's an important issue because of its wide range of applications in cementless joints, repair, and replacement of massive bone defects caused by various factors [1]. Bone disease and trauma are especially difficult to treat, especially in complex or large defects. The articular joint performs precise movements, bears compression, and is essential for mobility

*Corresponding author: hakgul@karabuk.edu.tr

and daily living activities [2]. Orthopedic implants provide huge benefits to the patient but have limited durability. Because of their limited lifespan and inability to grow with the patient, they are not recommended for younger patients. They can also fail to Osseo integrate and become aseptically loose. In patients aged 46-50, the risk of revision is greater than 25% [3]. Critical-sized bone defects, which are defined as those that will not heal spontaneously within a patient's lifetime, pose a significant threat to a patient's quality of life [4]. The use of autologous bone graft is the current best standard clinical material for bone regeneration [5]. A fully functional composite construct remains an elusive goal in the field of tissue engineering. Because it allows for a high degree of geometric control on both the macro- and micro-scales, 3D bioprinting is a promising new technology. It enables us to create patient-specific bioactive scaffolds using 3D imaging techniques like magnetic resonance imaging (MRI), computed tomography (CT), and positron emission tomography (PET) [6].

Selecting suitable material for 3D Bioprinting is an essential part of the work. Bone Scaffolds should serve 3 capabilities in tissue engineering applications. Firstly, are corporal parameters that require to identification the geometrical shape of the scaffold in particular its pore size and porosity. The second required parameter is to provide sufficient mechanical strength. Finally, the last parameter is to allow the cell implantation and at the same time biodegradation rate of the scaffold.

Scaffolds can be modeled using some architectural structures like honey-comb structures, circular, rectangular or gyroid structures. But we do not have to forget that, if architectures changed, pore size and porosity is also changed. Required pore size and porosity need to be maintained as it disturbs the scaffold's mechanical parameters. At the time pore size and porosity are responsible for the flow of nutrients and growth factors of bone. Kelvin architecture is taken into consideration as an open cellular structure and it is used to model the scaffold mainly due to its resemblance to cancellous or spongy bone [7].

In terms of improving the biomedical performance of Ti6Al4V alloys, copper was added to produce alloys with antibacterial functionality and better corrosion resistance, antimicrobial susceptibility, and cytocompatibility [8], or tantalum to produce alloys with tensile properties such as a lower elastic modulus [9]. Ti6Al4V is commonly used in the fabrication of prostheses; however, Ti6Al4V lacks biological functions that prevent infection and promote osseointegration at the prosthesis-bone interface [10,11]. Without a doubt, this is detrimental to implant survival time and the clinical effect of surgery [12,13]. As a result, surface modification of 3D-printed Ti6Al4V implants has recently emerged as a new focus [14]. Mineral coatings, such as Ca/P by microarc oxidation [15], were also developed on 3D-printed Ti6Al4V porous implants with lower cost and stable quality, but their promotion of bone ingrowth was far from satisfactory, limiting their clinical applications significantly [16].

PLA is a semi-crystalline or amorphous, rigid thermoplastic polymer. Other features of PLA produced by using plants rich in starch, such as corn, sugar cane, and wheat, are biocompatibility and biodegradability [17]. PLA compositions are used in surgical sutures to keep the wound together and provide support. Its use in controlled drug release systems has also become common [18]. PLA has received a lot of attention recently because of its excellent bioresorbability, improved biocompatibility, and biodegradability with nontoxic byproduct formation. PLA has a wide range of applications, including medical and food industries, such as antimicrobial product development, bone tissue engineering, 3D-printed scaffold fabrication, and surgical suturing, as well as drug carrier agents [19-22]. The only disadvantage of using PLA is its inability to facilitate cell attachment and proliferation due to its poor cellular attachment ability [23].

A few years ago, it was not quite realistic to achieve 3D bioprinting of perfectly functional artificial organs for implantation. But nowadays, we cannot denied that

bioprinting techniques have evolved significantly. It will be good if evolution way of three-dimensional bioprinting is looked in.

In 1984, Charles Hull invented stereolithography (SLA) for printing 3D objects from digital data, it was a first step and symbol the birth of 3D printing [24]. Bioprinting was first demonstrated in 1988 while Klebe using a standard Hewlett-Packard (HP) inkjet printer to deposit cells by cytoscribing technology [25]. In 1996, Forgacs and co-workers drew a conclusion that apparent tissue surface tension was the macroscopic manifestation of molecular adhesion between cells and provided a quantitative measure for tissue cohesion [26]. In 1999, Odde and Renn first utilized laser assisted bioprinting to deposit living cells for developing analogs with complex anatomy [27]. In 2001, direct printing of a scaffold in the shape of a bladder and seeding of human cells took place [28]. In 2002, the first extrusion-based bioprinting technology was reported by Landers et al., which was later commercialized as "3D-Bioplotter" [29]. Wilson and Boland developed the first inkjet bioprinter in 2003 by modifying an HP standard inkjet printer [30]. A year after, their team implemented cell-loaded bioprinting with a commercial SLA printer [31]. In the same year, 3D tissue with only cells (no scaffold) was developed. In 2006, electrohydrodynamic jetting was applied to deposit living cells [32]. Scaffold-free vascular tissue was engineered through bioprinting by Norotte et al. in 2009 [33]. In 2012, in situ bioprinting was attempted by Skardal et al. on mouse models [34]. The following years saw the introduction of many new bioprinting products, such as articular cartilage and artificial liver in 2012, tissue integration with circulatory system in 2014 and so on [35,36]. In 2015, coaxial technology was adopted by Gao et al. for fabrication of tubular structure [37]. In 2016, Pyo et al. applied rapid continuous optical 3D printing based on DLP [38]. In the same year, cartilage model was manufactured by Anthony Atala's research group using integrated tissue-organ printer (ITOP) [39]. In 2019, Noor et al. succeeded in manufacturing a perusable scale-down heart [40]. And a few months later, bioprinting of collagen human hearts at various scales based on freeform reversible embedding of suspended hydrogels (FRESH) technology was achieved by Lee et al [41]. A timeline for the evolution of bioprinting technology up to state-of-the-art is given in Table.1.

Table.1. A brief history of bioprinting

In 1980 years	In 1990 years	In 2000 years	In 2010 years	In 2019 year
1984, SLA was invented representing the birth of 3D printing.	1996, cell sticking together during embryonic development was observed.	2001, 3D printed synthetic scaffold for human ladder was achieved.	2012, *in situ* bioprinting was realized on animals.	2019, cardioid structure was first bioprinted in Tel Aviv University: collagen human heart at various scales was engineered using FRESH technology.
1988, bioprinting was first demonstrated by 2D micro-positioning of cells	1999, first use of laser technology demonstrating 2D patterning of living cells was reported.	2002, first extrusion-based bioprinter was used and further commercialized as "3D Bioplotter"	2015, tubular structure was printed by coaxial technology.	-

Continuation of table № 1

In 1980 years	In 1990 years	In 2000 years	In 2010 years	In 2019 year
-	-	2003, first inkjet bioprinter was developed by modifying an HP standard inkjet printer.	2016, rapid continuous optical 3D printing based on DLP was applied: cartilage model was obtained by ITOP system.	-
-	-	2004, 3D tissues with only cells (no scaffolds) was presented.	-	-
-	-	2009, scaffold-free vascular constructs were fabricated.	-	-

2 Objects and methods of research

PRISMA guidelines were used to conduct a systematic review of the literature using PubMed and Web of Science. Following that, full-text English language primary research articles published in the fields of bioengineering and regenerative medicine were filtered (Fig. 1). To find articles on cartilage, the search terms '((3D bio printed scaffold NOT (systematic review)) NOT (review)' were used. '(3d bio print osteochondral) NOT (review)' was used to find papers on the composite structure. as well as '(3d bio print Ti6Al4V and PLA scaffolds) NOT (review)'. To find bone construct articles, the search terms '(bioprinting OR "tissue printing") AND (bone OR osteo*)' were used. Using the terms '(((3d bioprinting) AND (extrusion)) AND ((blood) OR (vessel) OR (vasculature) OR (vascular)))', papers engineering vascular constructs were identified. Duplicate results were eliminated, and additional articles were discovered through references, resulting in a pool of primary articles for screening. Articles published prior to 2013, citations, reviews, short communications, case reports, articles written in languages other than English, and articles that did not meet the definition of 3DBP were excluded. Included were papers on 3D bioprinting of bone, scaffold, scaffold cartilage with bone (osteochondral), and Ti6Al4V alloys PLA matrix. AM strategies, as well as Ti6Al4V and PLA composites for individual constructs, were among the articles considered in this review. Descriptions of cells used, culture conditions, and materials for assembling structures were among the data extracted. Data from animal models was also included. Engineering characteristics and bio-similarity of the resulting construct were used to evaluate approaches.

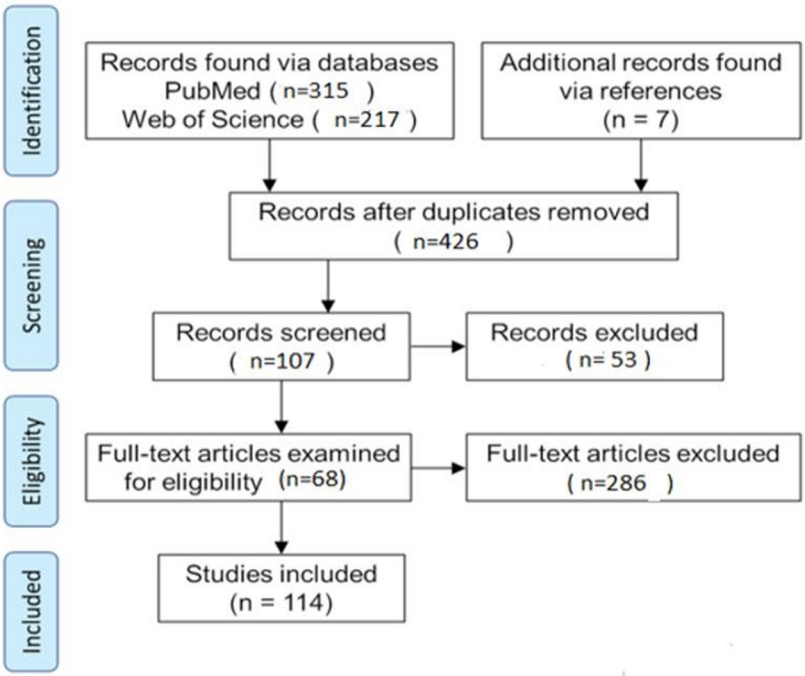

Fig. 1. PRISMA flow chart depicting article screening process

Excluded works include reviews, short communications, case reports, articles written in non-English languages, and articles which do not meet the definition of 3DBP. Example search terms include ((3D bioprint scaffolds NOT (systematic review)) NOT (review),

Figure 2 illustrates the findings of the SYRCLE's risk of bias analysis. The animal allocation sequence was adequate in 49 studies, and the baseline characteristics of the experimental animals were consistent across all studies. No study addressed whether the allocation was sufficiently concealed. According to only one study, the animals were housed at random. There was no explicit description of blind intervention or evaluation of outcomes. Because of the high cost of animals, the majority of studies (43 articles, 98%) did not choose animals at random for outcome assessment. Furthermore, many other items in the questionnaire were rated as "unclear," implying that the reporting of these studies (primarily experimental designs) needs to be improved.

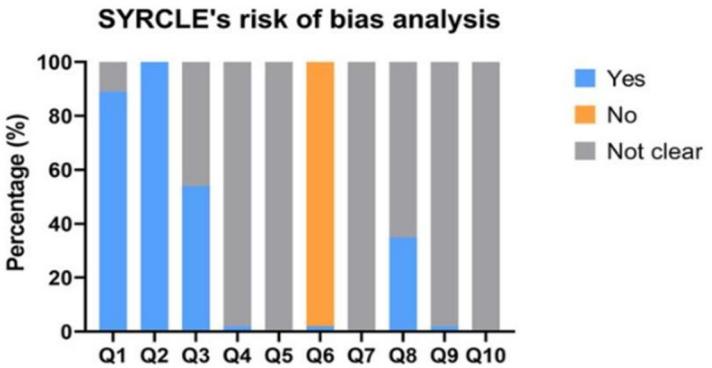

Fig. 2. Results of SYRCLE's risk of bias analysis

Figure 3 illustrates the CAMARADES checklist-assisted methodological quality assessment. The results of the article allocation, allocation concealment, and blind operation assessments were comparable to the results of the "risk of bias" assessment. Only one article mentioned the method for calculating sample size. The majority of studies (34 articles) clarified the use of relevant operating guidelines during experiments. Furthermore, the remainder of the items was rated as "unclear," which corresponded to the description in the "risk of bias" assessment.

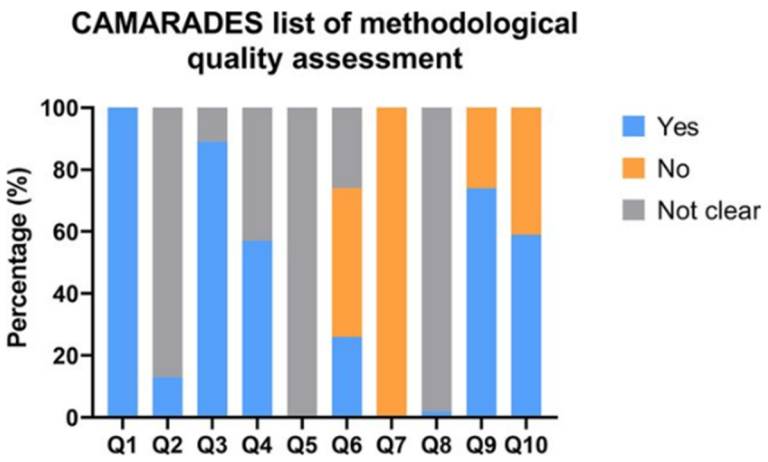

Fig. 3. Results of CAMARADES list of methodological quality assessment

Table 2 summarizes the design of the included articles. If an author's last name appeared in multiple articles, a number was added after the last name to differentiate the authors. A total of 29 studies mentioned the type of Ti6Al4V powder for 3D printing, with particle sizes ranging from 15 to 100 μm. In 16 studies, Grade 23 Ti6Al4V powder was incorporated. The 3D printing technique was mentioned in 44 studies which included; SLM, (26 studies, 59%), EBM (16 studies), and selective laser sintering (SLS) (2 studies,). Post-processing of the Ti64 scaffold was mentioned in 30 studies which involved removal of excess powder with either ultrasonic cleaning, sandblasting or acid treatment.

Most studies (40 studies) used a cylindrical scaffold, with the size varying depending on the animal model and reconstruction method. The strut size ranged from 60 to 3600 m, with the majority falling between 200 and 400 m. (20 studies,). The reported pore size ranged from 100-1500 m, with the majority of studies (23 studies) reporting a size of 500-700 m, followed by 300-499 m. (16 studies,). In 40 studies, the porosity of Ti64 scaffold ranged from 25 to; however, 60-70% was used in the majority of the studies (22 studies,). Depending on the unit cell used to design the lattice structure, different pore shapes could be observed, with some studies reporting on more than one pore shape. Diamond and the rhombic dodecahedron (8 studies).Other shapes included octahedrons, tetrahedrons, cubes, spiral tetrahedrons, hexagons, and cells based on triply periodic minimal surface (TPMS). The majority of studies (42 studies) used a regular lattice structure, whereas others used a randomly generated or arranged irregular pore structure [42, 49].

The randomly distributed pore structures in this review were classified as follows: 1. Pore structure designed using the Voronoi tessellation method [49]; 2. Pore structure designed using the TPMS model; 3. Randomly generated pore structure with varying pore

sizes and shapes [42]; 4. Regular shaped and regular-sized pore structure with randomly arranged pores [49, 50].

The mechanical strength of the Ti64 scaffold was reported in 15 studies, with values ranging from 14 to 606 MPa, with 10 studies describing it as having a strength between 30 and 200 MPa. The elastic modulus **ranged** from 0.32 to 7.56 GPa, with the majority of studies falling between 0 and 3GPa (12 studies,).

Table 2.

№	Researcher	Year	Host material	Composition (Addition)
1	Zhang et al	2021	Ti6Al4V	Bioactive glass and mesoporous bioactive glass coating
2	Ma et al.	2021	Ti6Al4V	Addition of gelatin methacrylate
3	Kelly et al	2021	Ti6Al4V	-
4	Chen et al.	2020	Ti6Al4V	-
5	Crovace et al.	2020	Ti6Al4V	-
6	Fan et al.	2020	Ti6Al4V	Barium titanate coating
7	Guo et al.	2020	Ti6Al4V	Titanium copper/ titanium copper nitride multilayer coating
8	Koolen et al	2020	Ti6Al4V	AlAcH treatment
9	Liu et al.	2020	Ti6Al4V	-
10	Lyu et al	2020	Ti6Al4V	-
11	Ragone et al.	2020	Ti6Al4V	-
12	Yu et al	2020	Ti6Al4V	-
13	Zhong et al	2020	Ti6Al4V	-
14	Mumith et al	2020	Ti6Al4V	HA coating, silicon-substituted or strontium- substituted HA coating
15	Bandyopadhyay	2019	Ti6Al4V	Anodization treat- ment
16	Chen et al	2019	Ti6Al4V	-
17	Gilev et al.	2019	Ti6Al4V	-
18	Li et al.	2019	Ti6Al4V	Polydopamine coating
19	Li et al.	2019	Ti6Al4V	-
20	Luan et al	2019	Ti6Al4V	-
21	Song et al	2019	Ti6Al4V	HA coating
22	Tanzer et al	2019	Ti6Al4V	HA coating
23	Tsai et al.	2019	Ti6Al4V	Magnesium–cal- cium silicate and chitosan coating
24	Guo et al.	2018	Ti6Al4V	-
25	Ma et al.	2018	Ti6Al4V	Addition of miner- alized collagen
26	Ran et al.	2018	Ti6Al4V	-
27	Wang et al.	2018	Ti6Al4V	-
28	Wang et al	2018	Ti6Al4V	Strontium ion incorporated zeolite coating
29	Huang et al	2017	Ti6Al4V	HA coating
30	Palmquist et al.	2017	Ti6Al4V	-
31	Xiu et al.	2017	Ti6Al4V	Hybrid micro-arc oxidation and hydrothermal treatment
32	Xiu et al.	2017	Ti6Al4V	Hybrid micro-arc oxidation
33	Arabnejad et al	2016	Ti6Al4V	-
34	Han et al	2016	Ti6Al4V	Anodization treatment and strontium incorpo- ration
35	Hara et al.	2016	Ti6Al4V	-
36	Li et al.	2016	Ti6Al4V	-

Continuation of table № 2

№	Researcher	Year	Host material	Composition (Addition)
37	Liu et al.	2016	Ti6Al4V	coating Addition of simvastatin and hydrogel
38	Shah et al	2016	Ti6Al4V	-
39	Shah et al.	2016	Ti6Al4V	-
40	Li et al.	2015	Ti6Al4V	Polydopamine- assisted hydroxyapatite
41	Lv et al.	2015	Ti6Al4V	Addition of bone morphogenetic protein-2 (BMP-2), vascular endothe- lial growth factor and fibringel
42	van der Stok et al.	2015	Ti6Al4V	AlAcH surface treatment and addition of BMP-2 and fibrin gel
43	van der Stok et al.	2015	Ti6Al4V	AlAcH surface treatment and osteostatin coat- ing
44	Yavari et al	2014	Ti6Al4V	Acid–alkali treat- ment, AlAcH treatment and anodizing-heat treatment
45	Palmquist et al.	2013	Ti6Al4V	-
46	van der Stok et al.	2013	Ti6Al4V	AlAcH treatment
47	Yavari et al	2014	Ti6Al4V	Acid–alkali treat- ment, AlAcH treatment and anodizing-heat treatment
48	Palmquist et al.	2013	Ti6Al4V	-
49	van der Stok et al.	2013	Ti6Al4V	

Continuation of table № 2

№	Fabrication method	Structure size (μm)	Scaffold shape and size (Ø * h, in mm	Porosity (%)	Animal	Biodegradation time (week)
1	SLM	300	C(5 * 10)	68	Rabbit	6-9
2	SLM	400	C(15 * 20)	76	Rabbit	4-12
3	SLM	-	C(4.5 * 8)	70	Rat	12
4	SLM	-	C(3 * 4)	60-70	Rat	4-12
5	EBM	-	C(12 * 400)	90	Sheep	48
6	EBM	382–383	C(5 * 13)	70-71	Rabbit	6-12
7	SLM	-	C(5 * 10)	70-75	Rabbit	4,8-12
8	SLS	211	C(5 * 6)	79	Rat	11
9	SLM	-	C(10 * 10)	65	Rabbit	4-12
10	-	320	C(2 * 5)	70	Rabbit	12
11	SLM	200	C(6.2 * 11)	75-90	Sheep	6,10-14
12	SLM	200	Cone-shape	90	Rabbit	4-8
13	SLM	-	C(6 * 10)	-	Rabbit	6-12
14	SLS	300-750	C(8 * 14.5)	70-75	Sheep	6
15	SLM	-	C(3 * 5)	25	Rat	12
16	SLM	300	C(6 * 6)	70	Dog	4-12
17	SLM	-	Cubic	-	Rabbit	1,2,6,12 and 48

Continuation of table № 2

№	Fabrication method	Structure size (μm)	Scaffold shape and size (Ø * h, in mm	Porosity (%)	Animal	Biodegradation time (week)
18	SLM	400	C(5 * 6)	45	Rabbit	5
19	SLM	-	C(8 * 10)	50	Pig	5
20	EBM	334-402	C(5 * 4)	55-78	Rabbit	12
21	SLM	341	C(3 * 6)	65-86	Rabbit	12-24
22	SLM	-	C(5.2 * 10)	50-65	Dog	-
23	SLM	350	C(6.5 * 10)	-	Rabbit	6
24	SLM	-	C(5 * 10)	74	Rabbit	4,8-12
25	SLM	-	C(5 * 6)	76	Rabbit	4-12
26	SLM	300-400	C(4 * 13)	-	Rabbit	4-12
27	SLM	410-449	C(4.8 * 8)	61-66	Rabbit	4-8
28	-	-	C(8 * 10)	-	Rabbit	4
29	EBM	238	C(10 * 20)	69	Goat	8-16
30	EBM	350	C(5.2 * 5)	70	Sheep	24
31	EBM	400	C(6 * 5)	73	Rabbit	8
32	EBM	400	C(6 * 5)	73	Rabbit	8
33	SLM	200-400	C(5 * 10)	56-70	Dog	4-8
34	EBM	400	C(5 * 5)	55-67	Rabbit	4-12
35	EBM	-	C(5 * 12)	65-70	Rabbit	4-12
36	EBM	200	C(10 * 30)	34	Goat	12,24-48
37	EBM	400	C(5 * 16)	76	Rabbit	4-8
38	EBM	583	C(5.2 * 7)	63	Sheep	24
39	EBM	341	C(5.2 * 5)	70	Sheep	26
40	EBM	-	C(5 * 10)	68	Rabbit	4-12
41	EBM	-	C(5 * 6)	-	Rabbit	4
42	SLM	165	Femur-shape	85	Rat	12
43	SLM	120	Femur-shape	88	Rat	12
44	SLM	160-180	Femur-shape	85-89	Rat	4,8-12
45	EBM	500-100	C(5.2 * 7)	-	Sheep	26
46		120	Femur-shape	-	Rat	4,8-12
47	SLM	160-180	Femur-shape	85-89	Rat	4,8-12
48	EBM	500-100	C(5.2 * 7)	-	Sheep	26
49	AlAcH treatment	120	Femur-shape	-	Rat	4,8-12

3 Results and their discussion

The initial search yielded 532 results. Based on the inclusion criteria, only 46 animal studies were found to be eligible. The rabbit was the most frequently used animal model. Pore sizes of 500-600 m and porosity of 60-70% were discovered to be the most ideal parameters for designing the Ti64 scaffold, with both dodecahedron and diamond pores promoting osteogenesis optimally. At weeks 8-10, histological analysis of the scaffold in a

rabbit model revealed that the maximum bone area fraction reached 59.38.1%. At week 12, the maximum bone volume fraction was found to be 34.06.0% using micro-CT analysis.

4 Conclusions

Ti64 scaffolding has the potential to be a promising medium for providing mechanical support and a stable environment for new bone formation in long bone defects. Furthermore, rhombic dodecahedron- or diamond-shaped pores with pore sizes of 500-700 m and porosities of 60-70% could be considered the most optimal parameters for scaffold manufacturing. More research is needed using large animal models and standardized protocols to extrapolate animal study results to humans for potential clinical applications. Ti64 scaffold might act as a promising medium for providing sufficient mechanical support and a stable environment for new bone formation in long bone defects.

References

1. Farazin, A., Zhang, C., Gheisizadeh, A., and Shahbazi, A. 3D bio-printing for use as bone replacement tissues: A review of biomedical application. Biomedical Engineering Advances, 100075. (2023).
2. Sugiura, H., and Demura, S. Effects of mild and severe knee joint pain on various activities of daily living in the female elderly. Pain Research and Treatment, (2013).
3. Nugent, M., Young, S. W., Frampton, C. M., and Hooper, G. J. The lifetime risk of revision following total hip arthroplasty: a new Zealand joint registry study. The bone and joint journal, 103(3), 479-485. (2021).
4. Reakasame, S., and Boccaccini, A. R. Oxidized alginate-based hydrogels for tissue engineering applications: a review. Biomacromolecules, 19(1), 3-21. (2018).
5. Roddy, E., DeBaun, M. R., Daoud-Gray, A., Yang, Y. P., and Gardner, M. J. Treatment of critical-sized bone defects: clinical and tissue engineering perspectives. European Journal of Orthopaedic Surgery and Traumatology, 28, 351-362. (2018).
6. Bittner, S. M., Smith, B. T., Diaz-Gomez, L., Hudgins, C. D., Melchiorri, A. J., Scott, D. W., and Mikos, A. G. Fabrication and mechanical characterization of 3D printed vertical uniform and gradient scaffolds for bone and osteochondral tissue engineering. Acta biomaterialia, 90, 37-48. (2019).
7. Sanas, M. M., and Mulay, A. V. Evaluating biological behavior of Kelvin cellular bone scaffold. Materials Today: Proceedings, 62, 32-36. (2022).
8. Guo, S., Lu, Y., Wu, S., Liu, L., He, M., Zhao, C., and Lin, J. Preliminary study on the corrosion resistance, antibacterial activity and cytotoxicity of selective-laser-melted Ti6Al4V-xCu alloys. Materials Science and Engineering: C, 72, 631-640. (2017).
9. Sing, S. L., Yeong, W. Y., and Wiria, F. E. Selective laser melting of titanium alloy with 50 wt% tantalum: Microstructure and mechanical properties. Journal of Alloys and Compounds, 660, 461-470. (2016).
10. Salvador, C. A., Maia, E. L., Costa, F. H., Escobar, J. D., and Oliveira, J. P. A compilation of experimental data on the mechanical properties and microstructural features of Ti-alloys. Scientific data, 9(1), 188. (2022).
11. Callegari, B., Oliveira, J. P., Aristizabal, K., Coelho, R. S., Brito, P. P., Wu, L., and Pinto, H. C. In-situ synchrotron radiation study of the aging response of Ti-6Al-4V alloy with different starting microstructures. Materials Characterization, 165, 110400. (2020).

12. Jing, Z., Zhang, T., Xiu, P., Cai, H., Wei, Q., Fan, D., and Liu, Z. Functionalization of 3D-printed titanium alloy orthopedic implants: A literature review. Biomedical Materials, 15(5), 052003. (2020).
13. Goodman, S. B., Yao, Z., Keeney, M., and Yang, F. The future of biologic coatings for orthopaedic implants. Biomaterials, 34(13), 3174-3183. (2013).
14. Sheng, X., Wang, A., Wang, Z., Liu, H., Wang, J., and Li, C. Advanced Surface Modification for 3D-Printed Titanium Alloy Implant Interface Functionalization. Frontiers in bioengineering and biotechnology, 10. (2022).
15. Xiu, P., Jia, Z., Lv, J., Yin, C., Cheng, Y., Zhang, K., Liu, Z. Tailored surface treatment of 3D printed porous Ti6Al4V by microarc oxidation for enhanced osseointegration via optimized bone in-growth patterns and interlocked bone/implant interface. ACS applied materials and interfaces, 8(28), 17964-17975. (2016).
16. Ni, R., Jing, Z., Xiong, C., Meng, D., Wei, C., and Cai, H. Effect of micro-arc oxidation surface modification of 3D-printed porous titanium alloys on biological properties. Annals of Translational Medicine, 10(12). (2022).
17. Evlen, H., and Erel, G. Effect of the Reinforcement Phase on the Mechanical and Biocompatibility Properties of PLA Matrix Nano Composites. Polym. Korea, 45(4), 491-500. (2021).
18. Salahuddin, N., Abdelwahab, M., Gaber, M., and Elneanaey, S. Synthesis and Design of Norfloxacin drug delivery system based on PLA/TiO2 nanocomposites: Antibacterial and antitumor activities. Materials Science and Engineering: C, 108, 110337. (2020).
19. Gong, M., Zhao, Q., Dai, L., Li, Y., and Jiang, T. Fabrication of polylactic acid/hydroxyapatite/graphene oxide composite and their thermal stability, hydrophobic and mechanical properties. Journal of Asian Ceramic Societies, 5(2), 160-168. (2017).
20. Liu, Z., Chen, Y., Ding, W., and Zhang, C. Filling behavior, morphology evolution and crystallization behavior of microinjection molded poly (lactic acid)/hydroxyapatite nanocomposites. Composites Part A: Applied Science and Manufacturing, 72, 85-95. (2015).
21. Du, X., Fu, S., and Zhu, Y. 3D printing of ceramic-based scaffolds for bone tissue engineering: an overview. Journal of Materials Chemistry B, 6(27), 4397-4412. (2018).
22. Mamatha, S., Biswas, P., Das, D., and Johnson, R. Fabrication of complex shaped ceramic articles from 3D printed polylactic acid templates by replication process. Ceramics International, 45(15), 19577-19580. (2019).
23. Ma, Z., Mao, Z., and Gao, C. Surface modification and property analysis of biomedical polymers used for tissue engineering. Colloids and Surfaces B: Biointerfaces, 60(2), 137-157. (2007).
24. Gu, Z., Fu, J., Lin, H., and He, Y. Development of 3D bioprinting: From printing methods to biomedical applications. Asian Journal of Pharmaceutical Sciences, 15(5), 529-557. (2020).
25. Klebe, R. J. Cytoscribing: a method for micropositioning cells and the construction of two-and three-dimensional synthetic tissues. Experimental cell research, 179(2), 362-373. (1988).
26. Foty, R. A., Pfleger, C. M., Forgacs, G., and Steinberg, M. S. Surface tensions of embryonic tissues predict their mutual envelopment behavior. Development, 122(5), 1611-1620. (1996).

27. Odde, D. J., and Renn, M. J. Laser-guided direct writing for applications in biotechnology. Trends in biotechnology, 17(10), 385-389. (1999).
28. Karzyński, K., Kosowska, K., Ambrożkiewicz, F., Berman, A., Cichoń, J., Klak, M., Wszoła, M. Use of 3D bioprinting in biomedical engineering for clinical application. Medical Studies/Studia Medyczne, 34(1), 93-97. (2018).
29. Landers, R., Hübner, U., Schmelzeisen, R., and Mülhaupt, R. Rapid prototyping of scaffolds derived from thermoreversible hydrogels and tailored for applications in tissue engineering. Biomaterials, 23(23), 4437-4447. (2002).
30. Wilson Jr, W. C., and Boland, T. Cell and organ printing 1: protein and cell printers. The Anatomical Record Part A: discoveries in molecular, cellular, and evolutionary biology, 272(2), 491-496. (2003).
31. Dhariwala, B., Hunt, E., and Boland, T. Rapid prototyping of tissue-engineering constructs, using photopolymerizable hydrogels and stereolithography. Tissue engineering, 10(9-10), 1316-1322. (2004).
32. Jayasinghe, S. N., Qureshi, A. N., and Eagles, P. A. M. Electrohydrodynamic jet processing: An advanced electric-field-driven jetting phenomenon for processing living cells. Small [Internet]. 2 (2): 216–9. (2006).
33. Norotte, C., Marga, F. S., Niklason, L. E., and Forgacs, G. Scaffold-free vascular tissue engineering using bioprinting. Biomaterials, 30(30), 5910-5917. (2009).
34. Skardal, A., Mack, D., Kapetanovic, E., Atala, A., Jackson, J. D., Yoo, J., and Soker, S. Bioprinted amniotic fluid-derived stem cells accelerate healing of large skin wounds. Stem cells translational medicine, 1(11), 792-802. (2012).
35. Duan, B. State-of-the-art review of 3D bioprinting for cardiovascular tissue engineering. Annals of biomedical engineering, 45, 195-209. (2017).
36. Dababneh, A. B., and Ozbolat, I. T. Bioprinting technology: a current state-of-the-art review. Journal of Manufacturing Science and Engineering, 136(6). (2014).
37. Gao, Q., He, Y., Fu, J. Z., Liu, A., and Ma, L. Coaxial nozzle-assisted 3D bioprinting with built-in microchannels for nutrients delivery. Biomaterials, 61, 203-215. (2015).
38. Pyo, S. H., Wang, P., Hwang, H. H., Zhu, W., Warner, J., and Chen, S. Continuous optical 3D printing of green aliphatic polyurethanes. ACS applied materials and interfaces, 9(1), 836-844. (2017).
39. Kang, H. W., Lee, S. J., Ko, I. K., Kengla, C., Yoo, J. J., and Atala, A. A 3D bioprinting system to produce human-scale tissue constructs with structural integrity. Nature biotechnology, 34(3), 312-319. (2016).
40. Noor, N., Shapira, A., Edri, R., Gal, I., Wertheim, L., and Dvir, T. 3D printing of personalized thick and perfusable cardiac patches and hearts. Advanced science, 6(11), 1900344. (2019).
41. Lee, A. R. H. A., Hudson, A. R., Shiwarski, D. J., Tashman, J. W., Hinton, T. J., Yerneni, S., Feinberg, A. W. 3D bioprinting of collagen to rebuild components of the human heart. Science, 365(6452), 482-487. (2019).
42. Tanzer, M., Chuang, P. J., Ngo, C. G., Song, L., and TenHuisen, K. S. Characterization of bone ingrowth and interface mechanics of a new porous 3D printed biomaterial: an animal study. The Bone and Joint Journal, 101(6_Supple_B), 62-67. (2019).
43. Huang, H., Lan, P. H., Zhang, Y. Q., Li, X. K., Zhang, X., Yuan, C. F., ... and Guo, Z. Surface characterization and in vivo performance of plasma-sprayed hydroxyapatite-coated porous Ti6Al4V implants generated by electron beam melting. Surface and Coatings Technology, 283, 80-88. (2015).

44. Guo, Y., Wu, J., Xie, K., Tan, J., Yang, Y., Zhao, S., and Hao, Y. Study of bone regeneration and osteointegration effect of a novel selective laser-melted titanium-tantalum-niobium-zirconium alloy scaffold. ACS Biomaterials Science and Engineering, 5(12), 6463-6473. (2019).
45. Guo, Y., Xie, K., Jiang, W., Wang, L., Li, G., Zhao, S., and Hao, Y. In vitro and in vivo study of 3D-printed porous tantalum scaffolds for repairing bone defects. Acs Biomaterials Science and Engineering, 5(2), 1123-1133. (2018).
46. Wu, S., Liu, X., Yeung, K. W., Liu, C., and Yang, X. Biomimetic porous scaffolds for bone tissue engineering. Materials Science and Engineering: R: Reports, 80, 1-36. (2014).
47. Hooijmans, C. R., Rovers, M. M., De Vries, R. B., Leenaars, M., Ritskes-Hoitinga, M., and Langendam, M. W. SYRCLE's risk of bias tool for animal studies. BMC medical research methodology, 14, 1-9. (2014).
48. Hooijmans, C. R., Rovers, M. M., De Vries, R. B., Leenaars, M., Ritskes-Hoitinga, M., and Langendam, M. W. SYRCLE's risk of bias tool for animal studies. BMC medical research methodology, 14, 1-9. (2014).
49. Ragone, V., Canciani, E., Arosio, M., Olimpo, M., Piras, L. A., von Degerfeld, M. M., and Dellavia, C. In vivo osseointegration of a randomized trabecular titanium structure obtained by an additive manufacturing technique. Journal of Materials Science: Materials in Medicine, 31, 1-11. (2020).
50. Wang, H., Su, K., Su, L., Liang, P., Ji, P., and Wang, C. The effect of 3D-printed Ti6Al4V scaffolds with various macropore structures on osteointegration and osteogenesis: A biomechanical evaluation. Journal of the mechanical behavior of biomedical materials, 88, 488-496. (2018).